Version of Record: https://www.sciencedirect.com/science/article/pii/S0191261519302449
Manuscript_ee7e0877920cbb65c6ef85a880d2863b

Optimal Traffic Control at Smart Intersections: Automated Network Fundamental Diagram

Mahyar Amirgholy [a,1], Mehdi Nourinejad [b,2], H. Oliver Gao [a,3]

[a] *School of Civil and Environmental Engineering, Cornell University, Ithaca, NY, 14853*
[b] *Department of Civil Engineering, York University, Toronto, ON, M3J1P3*

Abstract

Recent advances in artificial intelligence and wireless communication technologies have created great potential to reduce congestion in urban networks. In this research, we develop a stochastic analytical model for optimal control of communicant autonomous vehicles (CAVs) at smart intersections. We present the automated network fundamental diagram (ANFD) as a macro-level modeling tool for urban networks with smart intersections. In the proposed cooperative control strategy, we make use of the headway between the CAV platoons in each direction for consecutive passage of the platoons in the crossing direction through non-signalized intersections with no delay. For this to happen, the arrival and departure of platoons in crossing directions need to be synchronized. To improve system robustness (synchronization success probability), we allow a marginal gap between arrival and departure of the consecutive platoons in crossing directions to make up for operational error in the synchronization process. We then develop a stochastic traffic model for the smart intersections. Our results show that the effects of increasing the platoon size and the marginal gap length on the network capacity are not always positive. In fact, the capacity can be maximized by optimizing these cooperative control variables. We analytically solve the traffic optimization problem for the platoon size and marginal gap length and derive a closed-form solution for a normal distribution of the operational error. The performance of the network with smart intersections is presented by a stochastic ANFD, derived analytically and verified numerically using the results of a simulation model. The simulation results show that optimizing the control variables increases the capacity by 138% when the error standard deviation is 0.1s.

Keywords: communicant autonomous vehicles, cooperative traffic control, stochastic operational error, platoon size, inter-platoon headway, macroscopic fundamental diagram

1 Introduction

Autonomous vehicles are expected to be introduced to the consumer market in the near future. The artificial intelligence and wireless communication technologies embedded in these vehicles make “driving” more convenient and roads safer (Zhang and Ioannou, 2004; Van Arem et al, 2006; Fernandes and Nunes, 2011, 2012; Aria et al., 2016; Shabanpour et al., 2018). Improvement in the traffic condition, however, would be trivial in urban networks without upgrading conventional traffic control systems (Mahmassani, 2016). In this research, we propose a cooperative traffic control strategy for smart intersections to reduce congestion in urban networks.

The concept of self-driving vehicles was introduced in the 1930s. However, only recent advances in computation, communication, and automation technologies have made it feasible to realize the dream of autonomous vehicles. Currently, major car manufacturers, along with high technology companies, are making prototypes to be introduced by 2025 (Shi and Prevedouros, 2016; Kockelman et al., 2017). The radar-based autopilot technology of autonomous vehicles enables real-time monitoring of the environment and automatic independent actions on roads (Bose and Ioannou, 2003; Ni et al., 2010; Zohdy et al., 2015; Aria et al., 2016; Kockelman et al., 2017). In addition to autopilot technology, the capability of communicant autonomous vehicles (CAVs) to exchange information with both

[1] *E-mail address:* amirgholy@cornell.edu
[2] *E-mail address:* mehdi.nourinejad@lassonde.yorku.ca
[3] *E-mail address:* hg55@cornell.edu (Corresponding author)

predecessors and infrastructure, through vehicle-to-vehicle (V2V) and vehicle-to-infrastructure (V2I) communication technologies, respectively, enables cooperative traffic control in automated highways and networks (Bekiaris-Liberis et al., 2016; Shi and Prevedouros, 2016; Ghiasi et al., 2017; Lioris et al, 2017).

Cooperative traffic control can substantially increase the throughput of automated highways by safely increasing speed and decreasing the headway between the CAVs moving in platoons. (Fernandes and Nunes, 2011, 2012; Lam and Katupitiya, 2013; Roncoli et al., 2014; Ghiasi et al., 2017). Improving highway throughputs, however, increases network inflow as well, which can worsen the traffic condition in urban regions by overloading the network over the peaks, ultimately causing a complete gridlock (hypercongestion phenomenon). Hence, the overall performance of the integrated system of highways and urban networks can be improved by dynamically controlling the speed and size of CAV platoons in highways to keep network inflow optimized over time (Amirgholy et al., 2019). Overall, the limited capacity of urban networks is the main barrier to improving the traffic condition, even in interregional highways. In this research, we aim to improve network capacity by enabling cooperative traffic control at smart urban intersections.

For automated networks, we coordinate CAV platoons to safely pass through each other at non-signalized intersections with no interruption. For this to happen, the inter-platoon headway (the time gap between the passage of the rear bumper of the last vehicle in a platoon and the front bumper of the leader of the next platoon, from a reference point) in each direction needs to be sufficient for the safe passage of the consecutive platoons in the crossing direction. Thus, the effect of increasing the size of the platoons on the capacity of the network is not always positive, as opposed to the case in automated highways[4]. In this research, we maximize network capacity by optimizing platoon size (number of vehicles in each platoon) as one of the primary cooperative control variables of the system.

Network capacity largely depends on the precision and speed of sensors, computation processing, vehicle-to-vehicle and vehicle-to-infrastructure communication technology, and the actuation system. Operational error in coordinating the arrival and departure of the platoons at an intersection can cause a failure (interruption) in the synchronization process. For resynchronization, the approaching platoon stops at the intersection upon an early/late arrival and waits for the next upcoming spacing between the successive platoons (spacing between the rear bumper of the last vehicle in a platoon and the front bumper of the leader of the next platoon) in the crossing direction to pass through the intersection. In this case, the inter-platoon headway also needs to be adjusted for the safe passage of the stopped platoon through the intersection. When the synchronization process fails repeatedly, the capacity significantly drops. Hence, we maximize the network capacity by allowing a marginal gap (extra time gap) of an optimal length between the arrival and departure of the consecutive platoons in crossing directions.

In this research, we develop a stochastic analytical model for optimal traffic control at smart intersections. We formulate synchronization failure probability as a function of marginal gap length for a general statistical distribution of the operational error. We then derive the intersection capacity by accounting for the probabilistic impacts of synchronization failure. Our analytical results show that the intersection capacity can be maximized by optimizing the size of platoons and the length of the marginal gap. We analytically solve the optimal control problem for the platoon size and the marginal gap length and derive a closed-form solution for a general (bell-shaped) statistical distribution of the operational error. To show the generality of the analytical derivations, we also reformulate the closed-form solution for a normal distribution of the operation error. The performance of the network with smart intersections is also presented by the automated network fundamental diagram (ANFD). The stochastic ANFD reveals that the performance of the network in the "highly hypercongested" state can be improved by altering the pattern of the synchronized operation from approach-and-pass to stop-and-pass in one of the directions. In the end, we verify the analytical results using a double-ring simulation model. The simulation results show that optimizing the control variables increases the capacity by 138% when the error standard deviation is 0.1s.

The remainder of the paper is organized as follows: Section 2 develops a stochastic traffic model for the smart intersections. Section 3 formulates the optimal control problem. Section 4 presents the analytical ANFD. In Section

[4] In automated highways, the capacity is an increasing function of the platoon size (Varaiya, 1993; Michael et al., 1998; Fernandes and Nunes, 2012, 2015; Chen et al., 2017)

5, we evaluate the analytical model with the results of a simulation model. Lastly, conclusions of the paper are summarized in Section 6.

2 Cooperative Traffic Control in Automated Networks

Cooperative traffic control can substantially improve the performance of urban networks. On the link level, it improves capacity by safely increasing the speed and decreasing the headway between the CAVs moving in platoons. At intersections, the delay can be entirely eliminated by coordinating arrival and departure of platoons in crossing directions, as illustrated in Fig. 1.

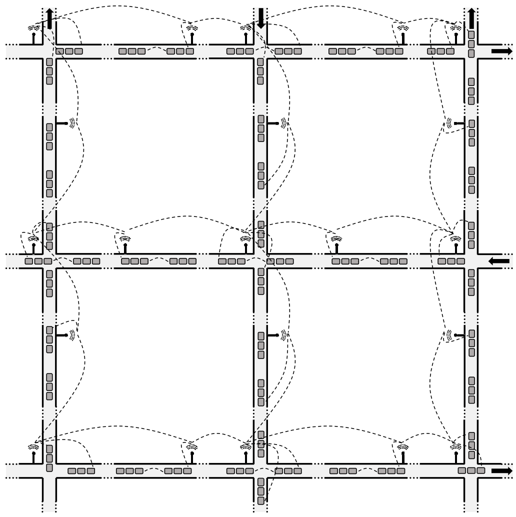

Fig. 1. Cooperative traffic control in automated networks

In the proposed cooperative control strategy, we make use of the spacing between successive platoons in each direction for the consecutive pass of the platoons in the crossing direction. For this to happen, an approaching platoon should be synchronized to arrive at the intersection when the departing platoon in the crossing direction has already cleared the intersection. Meanwhile, the time gap to the arrival of next approaching platoon should also be equal to or larger than the minimum time required for the safe maneuvering of the platoon through the intersection. The platoon arrival time to the intersection and the headway between the platoons, however, are both subject to an operational error, which can cause occasional interruptions in the synchronized (approach-and-pass) operation of the intersection. In this case, the platoon that arrives at the intersection early (when the departing platoon has not cleared the intersection) or late (when the time gap to the arrival of next approaching platoon is insufficient for the safe pass of the entire length of the platoon through the intersection) has to stop at the intersection. The synchronization failure requires some adjustments in the operation of the intersection for resynchronizing the platoons. In the adjustment operation (stop-and-pass), a late/early approaching platoon has to stop at the intersection and wait for the next upcoming spacing in the crossing direction to pass through. For this to happen, the inter-platoon headway in the crossing direction also needs to be adjusted for the safe passage of the entire length of the platoon (that starts moving from rest with a constant acceleration rate) through the intersection. The resynchronization adjustments, however, adversely affect the performance of the intersection if synchronization fails repeatedly. To reduce the failure probability, we allow a marginal gap between arrival and departure of the consecutive platoons in crossing directions to make up for the operational error. In the following section, we develop an analytical model for the intersection capacity by accounting for the probabilistic impacts of synchronization failure on the performance of the intersection. For simplicity of formulation, we consider the case of one-way intersections with no turning traffic; however, the model can be further generalized by synchronizing the platoons along the multilane roads and accounting for the passing time of various turning movements and the corresponding probabilities in the formulations.

2.1 Synchronized Operation: Approach-and-Pass Pattern

Platoon synchronization can entirely eliminate the queue and delay by using the spacing between the CAV platoons for the consecutive passing of these platoons by each other with no interruption. When synchronization is accurate, an approaching platoon in direction $i \in \{X, Y\}$ arrives at the intersection when the departing platoon in direction $j \in \{X, Y\}$, $i \neq j$, has already cleared the intersection, as illustrated in Fig. 2a.

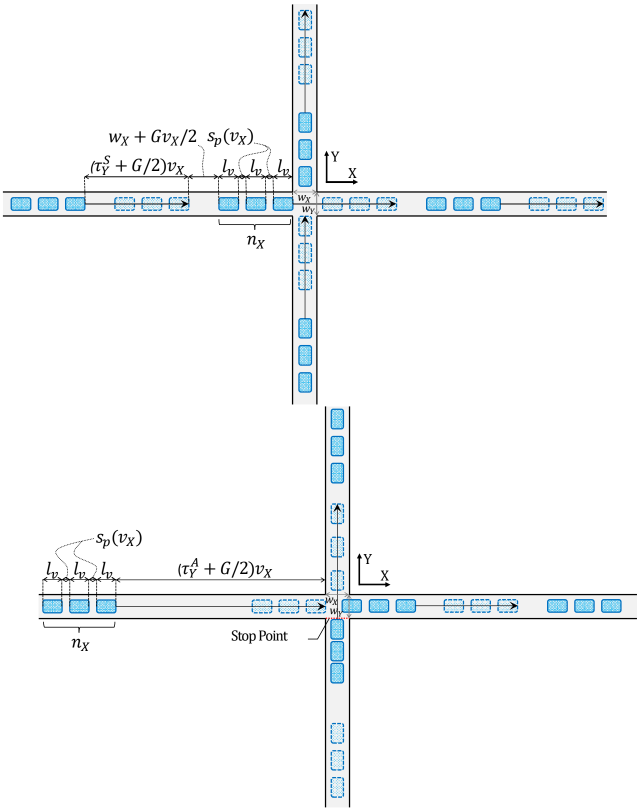

(a) Synchronized Operation (approach-and-pass) (b) Adjustment Operation (stop-and-pass)

Fig. 2. Cooperative traffic control at the smart intersections

We calculate the platoon passing time through the intersection in direction i, τ_i^S, as the required time for the entire length of a platoon of n_i vehicles to clear the intersection of width w_i with a constant speed of v_i:

$$\tau_i^S = \frac{n_i l_v + (n_i - 1)(\delta_o + \delta v_i) + w_i}{v_i}. \tag{1}$$

Here, the platoon length is the summation of the average vehicle length, l_v, and the intra-platoon spacing, s_p. The intra-platoon spacing is the bumper-to-bumper spacing between the vehicles in a platoon, expressed as a linear function of the speed with a constant buffer distance, i.e., intra-platoon jam spacing, δ_o (unit of length), and a fixed incremental rate, δ (unit of time): $s_p(v_i) = \delta_o + \delta v_i$. The clearance gap[5] is also calculated as w_i/v_i.

To improve the system robustness (synchronization success probability), we allow a marginal gap between arrival and departure of the consecutive platoons in crossing directions. By doing so, we reduce the probability of early/late arrivals at the intersection (synchronization failure probability), as we explain in Section 2.3. In a synchronized cycle, the arrival and departure of the consecutive platoons are successfully coordinated and platoons can approach and pass through the intersection with no interruption. The length of the synchronized cycle (time span required for the pass of one platoon in each of the directions), T^S, is equal to the summation of the platoon passing times through the intersection in crossing directions, τ_X^S and τ_Y^S, plus the marginal gap length, G, as shown in Fig. 3: $T^S = \tau_X^S + \tau_Y^S + G$.

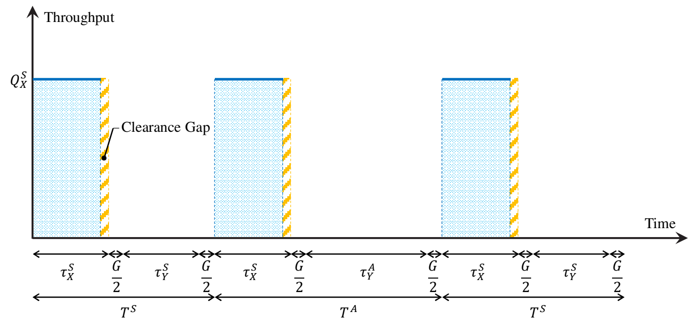

(a) Primary direction X

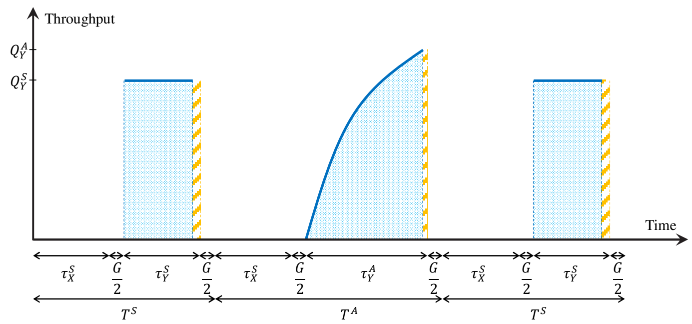

(b) Secondary direction Y

Fig. 3. Automated traffic flow profiles in crossing directions

The lane capacity (number of vehicles that pass through the intersection per lane per unit of time) in direction i, q_i^S, is then calculated as the platoon size in direction i, n_i, divided by the length of the synchronized cycle, T^S:

$$q_i^S = \frac{v_X v_Y}{(n_X v_Y + n_Y v_X) l_v + \big((n_Y - 1) v_X + (n_X - 1) v_Y\big)\delta_o + (n_X + n_Y - 2)\delta v_X v_Y + w_X v_Y + w_Y v_X + G v_X v_Y} n_i, \quad (2)$$

Here, indices i and j are substituted with X and Y in the first term of capacity function (2) since they are interchangeable. We further simplify the capacity function for the case of symmetric intersections ($n = n_X = n_Y$,

[5] Clearance gap refers to the extra time it takes a platoon to clear the intersection after the last vehicle of the platoon entered the intersection. By definition, the instantaneous throughput of the intersection is zero during the time a platoon is "clearing" the interstation, as graphically shown in the flow profiles of Fig. 3.

$v = v_X = v_Y$, $w = w_X = w_Y$) where the platoon passing times through the intersection become equal in crossing directions, $\tau^S = \tau_X^S = \tau_Y^S$:

$$q^S = \frac{nv}{2(nl_v + (n-1)(\delta_o + \delta v) + w) + Gv}. \quad (3)$$

The intersection capacity, in a synchronized cycle, is always a strictly increasing function of the speed and a strictly decreasing function of the marginal gap length, as the first-order (partial) derivatives of capacity function (3) with respect to v and G always have positive and negative values, respectively:

$$\frac{\partial q^S}{\partial v} = \frac{2n(nl_v + (n-1)\delta_o + w)}{(2(nl_v + (n-1)(\delta_o + \delta v) + w) + Gv)^2} > 0, \quad (4)$$

$$\frac{\partial q^S}{\partial G} = \frac{-nv^2}{(2(nl_v + (n-1)(\delta_o + \delta v) + w) + Gv)^2} < 0, \quad (5)$$

where $2n(nl_v + (n-1)\delta_o + w) > 0$ and $-nv^2 < 0$ for $\forall n \geq 1$ and $\forall v, l_v > 0$. The behavior of capacity function (3) with respect to the platoon size is also monotonic; however, its monotonicity depends on the marginal gap length. As graphically illustrated in Fig. 4a, the intersection capacity can be a strictly increasing, decreasing, or even a constant function of n under the following conditions:

$$\begin{cases} \dfrac{\partial q^S}{\partial n} > 0, & G > {G_S}^* \\ \dfrac{\partial q^S}{\partial n} = 0, & G = G_S^*, \\ \dfrac{\partial q^S}{\partial n} < 0, & G < G_S^* \end{cases} \quad (6)$$

where

$$\frac{\partial q^S}{\partial n} = \frac{(Gv - 2v\delta - 2\delta_o + 2w)v}{(2(nl_v + (n-1)(\delta_o + \delta v) + w) + Gv)^2}, \quad (7)$$

and G_S^* is the solution of the first-order condition equation, $\partial q^S / \partial n = 0$:

$$G_S^* = \frac{2(v\delta + \delta_o - w)}{v}. \quad (8)$$

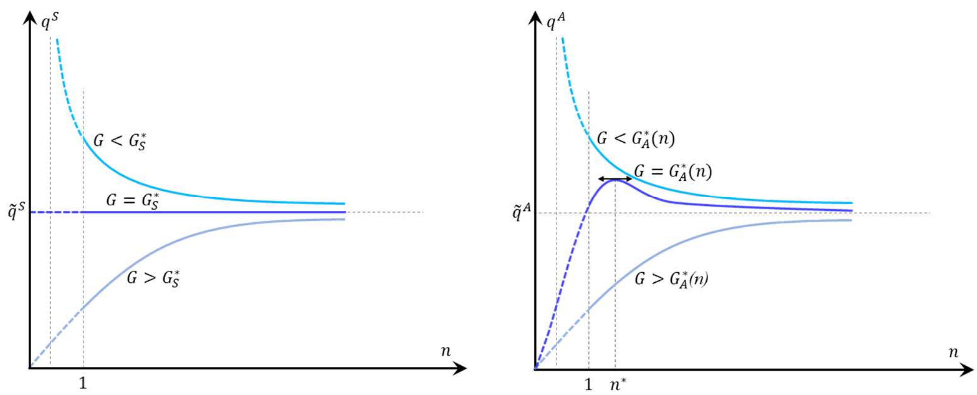

(a) Synchronized cycle (b) Adjustment cycle

Fig. 4. The capacity function behavior with respect to the platoon size

Note that the cycle length is an increasing function of the platoon size since the inter-platoon headway required for the safe pass of the consecutive platoons through each other at the intersection also increases with the platoon size. In a synchronized cycle, the effect of increasing the platoon size on the capacity is positive when $G > G_S^*$ in which case the cycle length grows slower than the platoon size ($\partial q^S/\partial n > 0$), negative when $G < G_S^*$ in which case the cycle length grows faster than the platoon size ($\partial q^S/\partial n < 0$), and neutral when $G = G_S^*$ in which case the cycle length and platoon size grow proportionally ($\partial q^S/\partial n = 0$). Although the effect of increasing the platoon size on the intersection capacity can be positive, negative, or neutral in a synchronized cycle, the limit value is fixed and independent of the platoon size and the marginal gap length in all the cases as the platoon size goes to infinity:

$$\tilde{q}^S = \lim_{n\to\infty} q^S = \frac{v}{2(l_v + v\delta + \delta_o)}. \tag{9}$$

2.2 Adjustment Operation: Stop-and-Pass Pattern

The operational error of the control system in coordinating the platoons causes a stochasticity in their platoon arrival times at the intersection. This error, if large enough, can cause an interruption in the synchronized (approach-and-pass) operation of the intersection (synchronization failure) when a platoon arrives at the intersection at the point in time that: (i) the departing platoon in the crossing direction has not cleared the intersection yet (early arrival), or (ii) the time gap to the arrival of the next approaching platoon in the crossing direction is insufficient for the safe passage of the platoon through the intersection (late arrival). Note that the concept of the earliness/lateness is by definition relative in the crossing directions; an early arrival in one direction can be also seen as a late departure in the crossing direction and vice versa. So, we choose a primary direction, X, as the reference, and define earliness/lateness in the secondary direction, Y. For resynchronization, the approaching platoon in direction Y stops at the intersection upon an early/late arrival, as illustrated in Fig. 2b. The stopped platoon then passes through the next upcoming spacing between the successive platoons in direction X with the maximum allowable acceleration rate[6], a_v. For this to happen, the inter-platoon headway in direction X also needs to be adjusted for the safe passage of the entire length of a platoon of n_Y vehicles in direction Y through the intersection of width w_Y, as described by the following equation of motion with constant acceleration from kinematics:

$$n_Y l_v + (n_Y - 1)\left(\delta_o + \delta\bar{v}_p(\tau_Y^A)\right) + w_Y = \frac{1}{2}a_v(\tau_Y^A)^2. \tag{10}$$

Note that the length of the passing platoon in direction Y continuously increases over time as the intra-platoon spacing increases with the rise in speed during the acceleration maneuver through the intersection. Here, the intra-platoon spacing is a linear function of the instantaneous speed, and the speed also increases linearly over time. Therefore, the platoon passing time through the intersection in secondary direction Y, τ_Y^A, can be equivalently derived for the average passing speed of the platoon, $\bar{v}_p(\tau_Y^A) = a_v\tau_Y^A/2$, by solving motion equation (10):

$$\tau_Y^A = \frac{a_v\delta(n_Y - 1) + c_1(n_Y)}{2a_v}, \tag{11}$$

with

$$c_1(n_Y) = \sqrt{\left(a_v\delta(n_Y - 1)\right)^2 + 8a_v(n_Y l_v + \delta_o(n_Y - 1) + w_Y)}\,, \tag{12}$$

where the term under the square root is positive for $\forall n_Y \geq 1$. The platoon passing time through the intersection in primary direction X, however, remains unchanged from the synchronized cycle, $\tau_X^A = \tau_X^S$, and can be derived using

[6] Maximum acceleration rate that is tolerable and safe for the passengers (see remarks of Li et al. (2014) and Le Vine et al. (2015)).

(1). In an adjustment cycle, we recalculate the passing time through the intersection in secondary direction Y for the case when a platoon has stopped at the intersection upon an early/late arrival. The length of the adjustment cycle (time span required for the passage of one platoon in each of the directions), T^A, is equal to the summation of the platoon passing times through the intersection in crossing directions, τ_X^S and τ_Y^A, plus the marginal gap length, G, as shown in Fig. 3: $T^A = \tau_X^S + \tau_Y^A + G$. The adjusted lane capacity in each direction $i \in \{\mathrm{X}, \mathrm{Y}\}$, q_i^A, is then derived as the size of the platoon (passes through the intersection per cycle) in direction i, n_i, divided by the length of the adjustment cycle, T^A:

$$q_i^A = \frac{2v_X a_v}{v_X c_1(n_Y) + c_2(n_X, n_Y) + 2v_X a_v G} n_i, \tag{13}$$

where

$$c_2(n_X, n_Y) = a_v(2n_X l_v + 2(n_X - 1)\delta_o + (2n_X + n_Y - 3)\delta v_X + 2w_X). \tag{14}$$

In a symmetric intersection, capacity function (13) is simplified as:

$$q^A = \frac{2nva_v}{vC_1(n) + C_2(n) + 2va_v G}, \tag{15}$$

where $C_1(n)$ and $C_2(n)$ are the symmetric versions of $c_1(n_Y)$ and $c_2(n_X, n_Y)$ in which n_i, v_i, and w_i are replaced by n, v, and w, respectively. Note that the adjustment operation causes a decline in the capacity of the intersection ($q^A \leq q^S$) since the cycle length increases in the adjustment cycles since $\tau^A \geq \tau^S$.[7]

Similar to a synchronized cycle, the intersection capacity in an adjustment cycle is also a strictly increasing and decreasing function of the speed and the marginal gap length, respectively:

$$\frac{\partial q^A}{\partial v} = \frac{4a_v^2 n(nl_v + \delta_o(n-1) + w)}{(vC_1(n) + C_2(n) + 2va_v G)^2} > 0, \tag{16}$$

$$\frac{\partial q^A}{\partial G} = \frac{-4a_v^2 nv^2}{(vC_1(n) + C_2(n) + 2va_v G)^2} < 0, \tag{17}$$

since $4a_v^2 n(nl_v + \delta_o(n-1) + w) > 0$ and $-4a_v^2 nv^2 < 0$ for $\forall n \geq 1$ and $\forall v, l_v, w > 0$. The behavior of the capacity function with respect to the platoon size, however, also depends on the parameters and variables other than the platoon size. As depicted in Fig. 4b, capacity model (15) can be a strictly increasing, decreasing, or even a non-monotonic function of the platoon size, n, under the following conditions:

$$\begin{cases} \dfrac{\partial q^A}{\partial n} > 0, & G > G_A^*(n) \\ \dfrac{\partial q^A}{\partial n} < 0, & G < G_A^*(n) \end{cases}, \tag{18}$$

where

---

[7] Theoretically, $\tau^A \geq \tau^S$ for $1 \leq n \leq n_U$ where $n_U = (2v^2 + a_v(\delta_o + \delta v - w))/(a_v(\delta_o + \delta v + l_v))$ is the solution of equation $\tau^A = \tau^S$ for $n \in \mathbb{R}_{>0}$. In practice, $n_U \geq 20$ for a reasonable range of values for the model variables and parameters, which is outranged by the platoon size safety/stability criteria (See the remarks of Biswas et al. (2006), Robinson et al. (2010), and Amoozadeh et al. (2015)), even in absence of an upper limit for the instantaneous speed of the platoons during the accelerating maneuver through the intersection.

$$\frac{\partial q^A}{\partial n} = \frac{2a_v v^2 \left(C_1(n) - \frac{n a_v (4(\delta_o + l_v) + a_v^2 \delta^2 (n-1))}{C_1(n)} \right) - (2\delta_o + 3\delta v - 2(Gv + w))}{(vC_1(n) + C_2(n) + 2va_vG)^2}, \quad (19)$$

and $G_A^*(n)$ is the solution of the first-order condition equation, $\partial q^A / \partial n = 0$:

$$G_A^*(n) = \frac{a_v \delta^2 (n-1) - 4(nl_v + \delta_o(n-2) + 2w)}{2C_1(n)} + \frac{\delta_o}{v} + \frac{3\delta}{2} - 2w. \quad (20)$$

The optimal platoon size in the non-monotonic case can be derived as:

$$n^* = G_A^{*-1}(G), \quad (21)$$

where $G_A^{*-1}(\cdot)$ denotes the inverse function of $G_A^*(\cdot)$.

In an adjustment cycle, increasing the platoon size causes the instantaneous speed of the platoon to further increase during the accelerating maneuver through the intersection as the platoon gets longer. Therefore, the overall effect of increasing the platoon size on the intersection capacity, in an adjustment cycle, is positive when $G > G_A^*(n)$, in which case the cycle length grows slower than the platoon size ($\partial q^A / \partial n > 0$), and negative when $G < G_A^*(n)$, in which case the cycle length grows faster than the platoon size ($\partial q^A / \partial n < 0$). In the non-monotonic case, however, the intersection capacity gets maximized at stationary point n^* where the cycle length varies proportionally with the platoon size so that the marginal effect of changing the platoon size on the intersection capacity becomes zero ($\partial q^A / \partial n = 0$). Although the intersection capacity can be a strictly increasing, decreasing, or even a non-monotonic function of the platoon size in an adjustment cycle, the limit value is fixed and independent of the platoon size and the marginal gap length in all these cases as the platoon size goes to infinity:

$$\tilde{q}^A = \lim_{n \to \infty} q^A = \frac{v}{l_v + 2v\delta + \delta_o}. \quad (22)$$

2.3 Synchronized Operation with a Probability of Failure

Interruption in the synchronized operation of the intersection, if it occurs repeatedly, can have negative impacts on the overall performance of the system. At the smart intersections, the robustness (success probability) of the control system (in coordinating the approach of the platoons in the crossing directions) can be significantly improved by allowing a marginal gap between arrival and departure of the consecutive platoons in crossing directions to reduce the failure probability at the cost of increasing the cycle length. In this case, an approaching platoon in direction Y can simultaneously pass through the intersection with no interruption in a synchronized cycle only if it arrives at the intersection within the marginal gap, after the departing platoon in direction X has cleared the intersection. However, an early/late platoon (one that arrives at the intersection before/after the marginal gap) has to stop at the intersection for resynchronization in an adjustment cycle.

To account for the stochasticity associated with the synchronization process, we consider a statistical distribution, with a general probability density function (PDF), f, for the random operational error in the platoon arrival time (with mean zero and standard deviation σ_ε) and the marginal gap length (with mean $\bar{G}$ and standard deviation σ_G): $\varepsilon \sim f(t; 0, \sigma_\varepsilon^2)$ and $G \sim f(t; \bar{G}, \sigma_G^2)$. The operational error generally has a symmetric[8] (bell-shaped) statistical distribution and the mean error in the coordinated arrival time of the platoons at the intersection is zero. Hence, the synchronization failure probability can be equally minimized for the early and late arrivals by coordinating the platoons to arrive to the intersection right at the midpoint of the marginal gap, with mean length of $\bar{G}$, as illustrated

[8] A probability distribution is symmetric if and only if $\exists x_o \mid f(x_o - \Delta) = f(x_o + \Delta),\ \forall \Delta \in \mathbb{R}$.

in Fig. 3a, b. In this case, the maximum success probability of the synchronized process, $\Pr(-G/2 \leq \varepsilon \leq G/2)$, can be formulated in terms of $\bar{G}$, as shown in Fig. 5:

$$P_s(\bar{G}) = \int_{-\bar{G}/2}^{\bar{G}/2} z(\omega)d\omega = Z\left(\frac{\bar{G}}{2}\right) - Z\left(-\frac{\bar{G}}{2}\right). \tag{23}$$

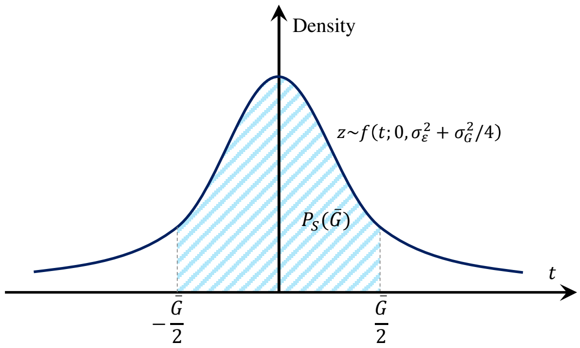

Fig. 5. General probability distribution of the operational error

Here, Z denotes the cumulative distribution of $z \sim f(t; 0, \sigma_\varepsilon^2 + \sigma_G^2/4)$. The probability of the synchronization failure (followed by the adjustment operation) is the complementary probability of success, $1 - \Pr(-G/2 \leq \varepsilon \leq G/2)$:

$$P_A(\bar{G}) = 1 - P_s(\bar{G}) = 1 + Z\left(-\frac{\bar{G}}{2}\right) - Z\left(\frac{\bar{G}}{2}\right). \tag{24}$$

The expected length of the cycles is calculated as the summation of the lengths of the synchronized and adjustment cycles, weighted by the success and failure probabilities: $\mathrm{E}[T] = T^S P_S(\bar{G}) + T^A P_A(\bar{G})$. The expected capacity in direction $i \in \{\mathrm{X}, \mathrm{Y}\}$ is then formulated as the size of the platoon (passes through the intersection per cycle) in direction i, n_i, divided by the expected length of the cycles, $\mathrm{E}[T]$:

$$q_i = \frac{n_i}{\tau_X^S P_S(\bar{G}) + \tau_X^A P_A(\bar{G}) + \tau_Y^S + \bar{G}}. \tag{25}$$

Here, τ_i^S and τ_X^A can be plugged in from (1) and (11), respectively. In a symmetric intersection, capacity model (23) is simplified as:

$$q = \frac{2nva_v}{(C_2(n) - vC_1(n) - 2a_v(n-1)\delta v)P_s(\bar{G}) + vC_1(n) + C_2(n) + 2va_v\bar{G}}. \tag{26}$$

As is the case in both synchronized and adjustment cycles, the expected capacity is also a stictly increasing function of speed, $\partial q/\partial v > 0$ for $\forall n \geq 1$ and $\forall v, l_v, w > 0$. The behavior of the capacity function with respect to the platoon size also follows a pattern similar to that of the adjustment cycle, while the limit value can be recalculated for the stochastic case as:

$$\tilde{q} = \lim_{n\to\infty} q = \frac{v}{2v\delta + (\delta_o + l_v)(1 + P_S(\bar{G}))}. \tag{27}$$

The intersection capacity, however, is not a monotonic function of the marginal gap length anymore when the synchronization process is subject to probabilistic failure. In the next section, we maximize the expected capacity of the intersection by optimizing the two primary control variables of the system: platoon size and marginal gap length.

3 Optimal Platoon Control Problem

Besides the physical and technological characteristics of the vehicles, infrastructure, and the control system, the intersection capacity largely depends on adjustments of the control system settings. To achieve the highest performance of the system, we maximize the expected capacity of the intersection by solving the following optimization problem for the platoon size, n, and the marginal gap mean length, $\bar{G}$:

$$\max_{n,\bar{G}} q = \frac{n}{\tau^S\big(1 + P_S(\bar{G})\big) + \tau^A P_A(\bar{G}) + \bar{G}}, \tag{28}$$

where $P_A(\bar{G}) = 1 - P_S(\bar{G})$, and τ^S and τ^A can be plugged in from relations (1) and (11), respectively, by replacing n_i, v_i, and w_i with n, v, and w for a symmetric intersection. The expected capacity is directly proportional to the platoon size, and inversely proportional to the expected cycle length, which is an increasing function of the platoon size. Therefore, the overall effect of increasing the platoon size on the expected capacity is positive for smaller platoons when the cycle length still grows slower than the platoon size ($\partial q/\partial n > 0$), and becomes negative for larger platoons when the cycle length grows faster than the platoon size ($\partial q/\partial n < 0$). So, the intersection capacity is maximized at stationary point n^* where the cycle length varies proportionally with the platoon size, where the marginal effect of a change in the platoon size on the intersection capacity becomes zero. Therefore, the size of the platoons can be optimized by solving the first-order condition equation ($\partial q/\partial n = 0$) for n as:

$$n^* = \frac{\left(\big(a_v\delta^2 - 4(\delta_o + l_v)\big)\left(2\big(1 - P_S(\bar{G})\big)^2 v^2(\delta_o - w) + C_3(\bar{G})\right) + \sqrt{2C_4(\bar{G})}\right)}{\big(a_v\delta^2 - 2(\delta_o + l_v)\big)\left(2\big(1 - P_S(\bar{G})\big)^2 v^2(\delta_o + l_v) + a_v\delta^2 C_3(\bar{G})\right)}, \tag{29}$$

where

$$C_3(\bar{G}) = \big(a_v(\delta_o + \delta v - w)\big(1 + P_S(\bar{G})\big) - \bar{G}v\big)\left((\delta_o - w)\big(1 + P_S(\bar{G})\big) - \bar{G}v + 2\delta v\right), \tag{30}$$

and

$$C_4(\bar{G}) = a_v\big(2(\delta_o + l_v)^2 - a_v\delta^2(l_v + w)\big)\left(2\delta_o\big(1 + P_S(\bar{G})\big) + \delta v\big(3 + P_S(\bar{G})\big) - 2\left(\bar{G}v + w\big(1 + P_S(\bar{G})\big)\right)\right)^2 \times \left(2\big(1 - P_S(\bar{G})\big)^2 v^2(\delta_o - w) + C_3(\bar{G})\right). \tag{31}$$

A marginal gap between arrival and departure of the platoons in crossing directions can significantly enhance the robustness (success probability) of the synchronization process at the cost of increasing the cycle length. Hence, the expected capacity of the intersection is maximized by allowing a marginal gap of an optimal length between arrival and departure of the consecutive platoons to make up for the associated operational error. In this case, the improvement resulting from the enhancement of robustness maximally outweighs the decline in the throughput of the intersection. Note that the success probability, $P_S(\bar{G})$, is generally an increasing concave function of $\bar{G} \geq 0$, regardless of type of the operational error distribution. Therefore, $\tau = \tau^S\big(1 + P_S(\bar{G})\big) + \tau^A\big(1 - P_S(\bar{G})\big)$ becomes a decreasing convex function of $\bar{G}$ since $\tau^A \geq \tau^S$. Following from above, $\mathrm{E}[T] = \tau + \bar{G}$ becomes a non-monotonic convex function of $\bar{G} \geq 0$, as illustrated in Fig. 6. The marginal gap (mean) length is then optimized by solving the following equation resulting from the first-order condition for the minimum expected cycle length, $\partial \mathrm{E}[T]/\partial \bar{G} = 0$:

$$\frac{\partial P_S(\bar{G})}{\partial \bar{G}}(\tau^A - \tau^S) - 1 = 0, \tag{32}$$

where

$$\frac{\partial P_s(\bar{G})}{\partial \bar{G}} = \frac{\partial\left(Z\left(\frac{\bar{G}}{2}\right) - Z\left(-\frac{\bar{G}}{2}\right)\right)}{\partial \bar{G}} = \frac{1}{2}\left(z\left(\frac{\bar{G}}{2}\right) + z\left(-\frac{\bar{G}}{2}\right)\right). \tag{33}$$

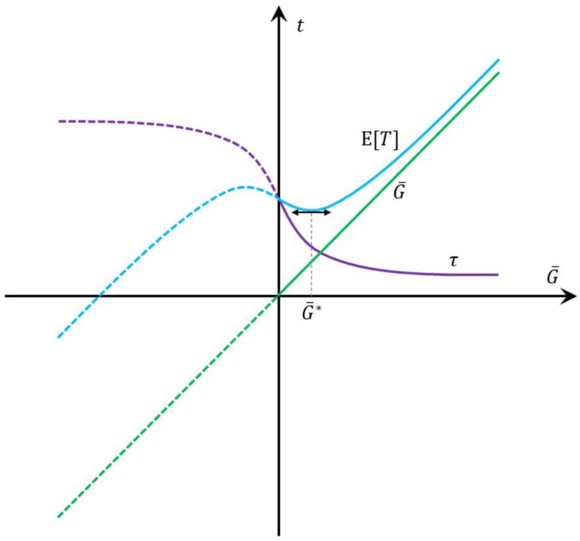

Fig. 6. Variations of the components of the expected cycle length with the marginal gap length ($\bar{G}$)

Since the operational error generally has a symmetric probability distribution, $z(\bar{G}/2) = z(-\bar{G}/2)$, relation (33) can be further simplified as:

$$\frac{\partial P_s(\bar{G})}{\partial \bar{G}} = z\left(\frac{\bar{G}}{2}\right). \tag{34}$$

By solving the equation resulting from plugging $\partial P_S(\bar{G})/\partial \bar{G}$ from relation (34) into first-order condition (32), the optimal marginal gap length, $\bar{G}^*$, is generally derived for any given parametric/nonparametric probability distribution of the operational error as:

$$\bar{G}^* = 2z^{-1}\left(\frac{1}{\tau^A - \tau^S}\right), \tag{35}$$

where $z^{-1}(\cdot)$ denotes the inverse function of $z \sim f(t; 0, \sigma_\varepsilon^2 + \sigma_G^2/4)$. Note that a closed-form solution can be simply generated for any invertible PDF of the operational error by substituting $z^{-1}(\cdot)$ in equation (35). To demonstrate the generality of the analytical derivations, we also reformulate the closed-form solution for a normal distribution of the operational error, $z \sim N(t; 0, \sigma_\varepsilon^2 + \sigma_G^2/4)$, which is a well-fitted statistical distribution for the operational error (Zito et al., 1995; Dulman et al, 2003; Yan and Bitmead, 2005):

$$\bar{G}^* = \sqrt{8(\sigma_\varepsilon^2 + \sigma_G^2/4)\ln\left(\frac{\tau^A - \tau^S}{\sqrt{2\pi(\sigma_\varepsilon^2 + \sigma_G^2/4)}}\right)}. \tag{36}$$

Optimizing the operation of the smart intersections can significantly improve the performance of the system at the network level, as we explain in Section 4.

4 Automated Network Fundamental Diagram

In this section, we present the automated network fundamental diagram (ANFD) as an analytical tool for modeling the dynamics of traffic in networks with smart intersections. In conventional networks, the macroscopic fundamental diagram (MFD) approximates the interrelationship between traffic variables in large urban regions. Observed traffic data from the city of Yokohama (Geroliminis and Daganzo, 2008) and the results of the traffic simulation of the downtown network of San Francisco (Geroliminis and Daganzo, 2007) show that when congestion has a uniform distribution across the network, flow (veh/s.lane) increases with vehicular density (veh/m.lane) from zero to its maximum value in the uncongested state of the network. The flow, however, sharply decreases with a further rise in density in the hypercongested state of the network until complete gridlock occurs (Daganzo, 2007; Daganzo and Geroliminis, 2008). In automated networks, cooperative traffic control makes it possible to keep the vehicular density homogenous across the network. The synchronization failure probability also remains identical for the intersections controlled by the same technology. The proposed analytical model for the intersection capacity can be then extended to present the performance of automated networks on a macroscopic level.

In networks with smart intersections, flow increases from zero to the network capacity with a rise in density in the uncongested state with no decline in the (free flow) speed, v. Further increase of the vehicular density, however, requires reducing the network speed to enable a further decrease of (i) the required inter-platoon spacing and (ii) the safe intra-platoon spacing in order to accommodate a larger number of platoons in the network. In this case, the network flow decreases with the decline of speed in the hypercongested state of the network as the system moves towards a complete gridlock. The ANFD expresses the relationship between the network flow, Q, and the vehicular density, k, in automated networks as shown below:

$$Q(k) = \begin{cases} kv, & 0 \le k \le k_m \\ kv(k), & k_m < k \le k_j \end{cases}, \tag{37}$$

where the optimal density, k_m, (for a given platoon size and marginal gap length) is calculated by plugging the network lane capacity from equations (3), (15), and (26) into Q_m in the macroscopic flow equation, $k_m = Q_m/v$, for approach-and-pass (absolute robust synchronization), stop-and-pass (absolute fragile synchronization), and stochastic (synchronization with a probability of failure) operation scenarios as shown below:

$$k_m = \begin{cases} \dfrac{n}{2(nl_v + (n-1)(\delta_o + \delta v) + w) + \bar{G}v} & \text{approach} - \text{and} - \text{pass} \\ \dfrac{2na_v}{vC_1(n) + C_2(n) + 2va_v\bar{G}} & \text{stop} - \text{and} - \text{pass} \\ \dfrac{2na_v}{(C_2(n) - vC_1(n) - 2a_v(n-1)\delta v)P_s(\bar{G}) + vC_1(n) + C_2(n) + 2va_v\bar{G}} & \text{stochastic} \end{cases}. \tag{38}$$

The network speed in the hypercongested state ($k_m < k \le k_j$) is then derived for different operation scenarios by reversing the optimal density function, $v(k) = k_m^{-1}(k)$:

$$v(k) = \begin{cases} \dfrac{n - 2k(nl_v + (n-1)\delta_o + w)}{k(2(n-1)\delta + \bar{G})} & \text{approach} - \text{and} - \text{pass} \\ \dfrac{2na_v - 2ka_v(nl_v + (n-1)\delta_o + w)}{k\big(3a_v(n-1)\delta + 2a_v\bar{G} + C_1(n)\big)} & \text{stop} - \text{and} - \text{pass} \\ \dfrac{2na_v - 2ka_v(nl_v + (n-1)\delta_o + w)\big(1 + P_s(\bar{G})\big)}{k\Big(a_v(n-1)\delta\big(3 + P_s(\bar{G})\big) + 2a_v\bar{G} + C_1(n)\big(1 - P_s(\bar{G})\big)\Big)} & \text{stochastic} \end{cases}. \tag{39}$$

The jam density in different operation scenarios is also derived by solving the zero speed equation, $v(k) = 0$:

$$k_j = \begin{cases} \dfrac{n}{2(nl_v + (n-1)\delta_o + w)} & \text{approach} - \text{and} - \text{pass} \\ \dfrac{n}{nl_v + (n-1)\delta_o + w} & \text{stop} - \text{and} - \text{pass} \\ \dfrac{n}{(nl_v + (n-1)\delta_o + w)\big(1 + P_s(\bar{G})\big)} & \text{stochastic} \end{cases}. \tag{40}$$

As illustrated in Fig. 7a, the ANFD is bounded from above and below by its extreme cases, while the failure probability, $P_A(\bar{G}) = P_s(\bar{G}) - 1$, varies between 0 and 1. The capacities derived for the network under the absolute robustness ($P_S(\bar{G}) = 1$ for $\forall \bar{G} \geq 0$) and absolute fragility ($P_S(\bar{G}) = 0$ for $\forall \bar{G} \geq 0$) conditions, respectively, determine the upper bound, Q_m^S, and the lower bound, Q_m^A, of the operational capacity of the network, $Q_m^A < Q_m < Q_m^S$, when the synchronization process at the intersections is subject to a probabilistic failure ($0 < P_S(\bar{G}) < 1$). For a given distribution of the operational error, the network capacity can be maximized by optimizing the size of the platoons, n, and the length of the marginal gaps, $\bar{G}$, as explained in Section 3. By plugging n^* and $\bar{G}^*$ from equations (29) and (35) into (38), the maximum achievable capacity of the network under stochasticity, Q_m^*, is derived for the adjusted optimal density, k_m^*, as shown in the optimal-hybrid ANFD of Fig. 7b. In automated networks, the jam density also varies between an upper bound and a lower bound when the operational error has a statistical distribution. In this case, the jam density derived under the absolute fragility condition ($P_S(\bar{G}) = 1$ for $\forall \bar{G} \geq 0$), k_j^A, determines the upper bound and the jam density derived under the absolute robustness condition ($P_S(\bar{G}) = 0$ for $\forall \bar{G} \geq 0$), k_j^S, determines the lower bound of the operational jam density in automated networks, $k_j^S < k_j < k_j^A$.

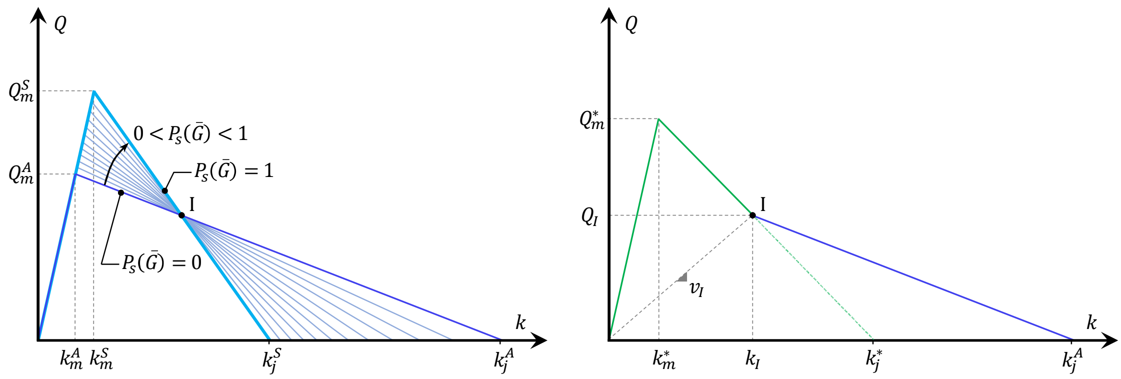

(a) Stochastic ANFD (b) Optimal-hybrid ANFD

Fig. 7. Automated network fundamental diagram (ANFD)

Remark. The performance of the network in the highly hypercongested state ($k > k_I$) can be significantly improved by altering the synchronized operation pattern of the intersections from approach-and-pass to stop-and-pass in one of the directions, as shown in Fig. 7b. The accelerating maneuver of the platoons through the intersections in the stop-and-pass operation scenario allows further increase of the density in the highly hypercongested state by reducing the minimum required inter-platoon spacing in comparison to the approach-and-pass operation scenario.

The critical density at interchange point I, k_I, is derived by solving the equation resulting from equating the upper and the lower bounds of the ANFD's declining legs:

$$k_I = \frac{n(C_1(n) - a_v(n-1)\delta)}{2(nl_v + (n-1)\delta_o + w)\Big(a_v\big((n-1)\delta + \bar{G}\big) + C_1(n)\Big)}. \tag{41}$$

The critical speed, $v_I = v(k_I)$, and flow, $Q_I = v_I k_I$ can be accordingly calculated at point I as:

$$v_I = \frac{1}{4}\left(a_v(n-1)\delta + C_1(n)\right), \tag{42}$$

$$Q_I = \frac{a_v n}{a_v\left((n-1)\delta + \bar{G}\right) + C_1(n)}. \tag{43}$$

Note that the performance of the system can be maximized by keeping the vehicular density of the network optimized over time using the dynamic perimeter control and demand management strategies introduced in the MFD literature (see remarks of Geroliminis and Levinson, 2009; Geroliminis et al., 2013; Ramezani et al., 2015; Amirgholy and Gao, 2017).

5 Simulation and Numerical Analysis

In this section, we evaluate the analytical model with the results of a simulation model. We also numerically evaluate the effects of adjusting the control system settings on the performance of the automated network. In this simulation, we use the double-ring concept developed by Daganzo et al. (2011). In this example, the average vehicle length is $l_v = 2$m, the maximum allowable acceleration rate is $a_v = 16\text{m/s}^2$, and the intersection width is $w = 3$m. In the absence of automation technology, the performance of a conventional (non-automated) system with a free flow speed[9] of $25\ \text{m/s}$ is presented by the MFD of Fig. 8.

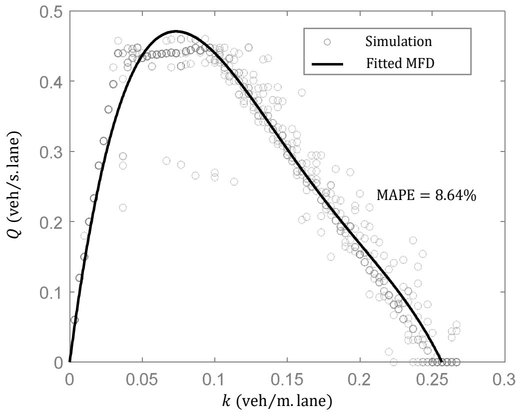

Fig. 8. Macroscopic fundamental diagram of the non-automated double-ring system

In automated networks, cooperative traffic control enables CAVs to safely move in close distane from their predecessors in platoons. Here, we calculate the intra-platoon spacing in a connected environment for fixed and variable incremental safety distance coefficients of $\delta_o = 0.1$m and $\delta = 0.4$s. Fig. 9a-f evaluate the analytical ANFD with the results of the double-ring simulation for a platoon size of $n = 3$, marginal gap length of $\bar{G} = 0.8$s, at different system accuracy levels, where the operational error has a normal distribution, $z \sim N(t; 0, \sigma_z^2)$. The results show that the analytical ANFD has a high accuracy, i.e., low mean absolute percentage error (MAPE), in approximating the macroscopic retaliation between flow (Q) and density (k) of automated networks. Comparing the

[9] CACC technology allows for a safe increase of the free flow speed in automated networks by reducing perception-reaction time. However, to evaluate the effects of automating the operation of traffic on the performance of the system, we use comparable simulation settings, including an identical free flow speed of $25\ \text{m/s}$ ($90\ \text{km/hr}$), for both conventional and automated double-ring systems.

simulation results of Fig. 8 and Fig. 9a-f shows that the proposed cooperative control strategy improves the capacity by 81% to 104%, depending on the accuracy of the control system in coordinating the platoons.

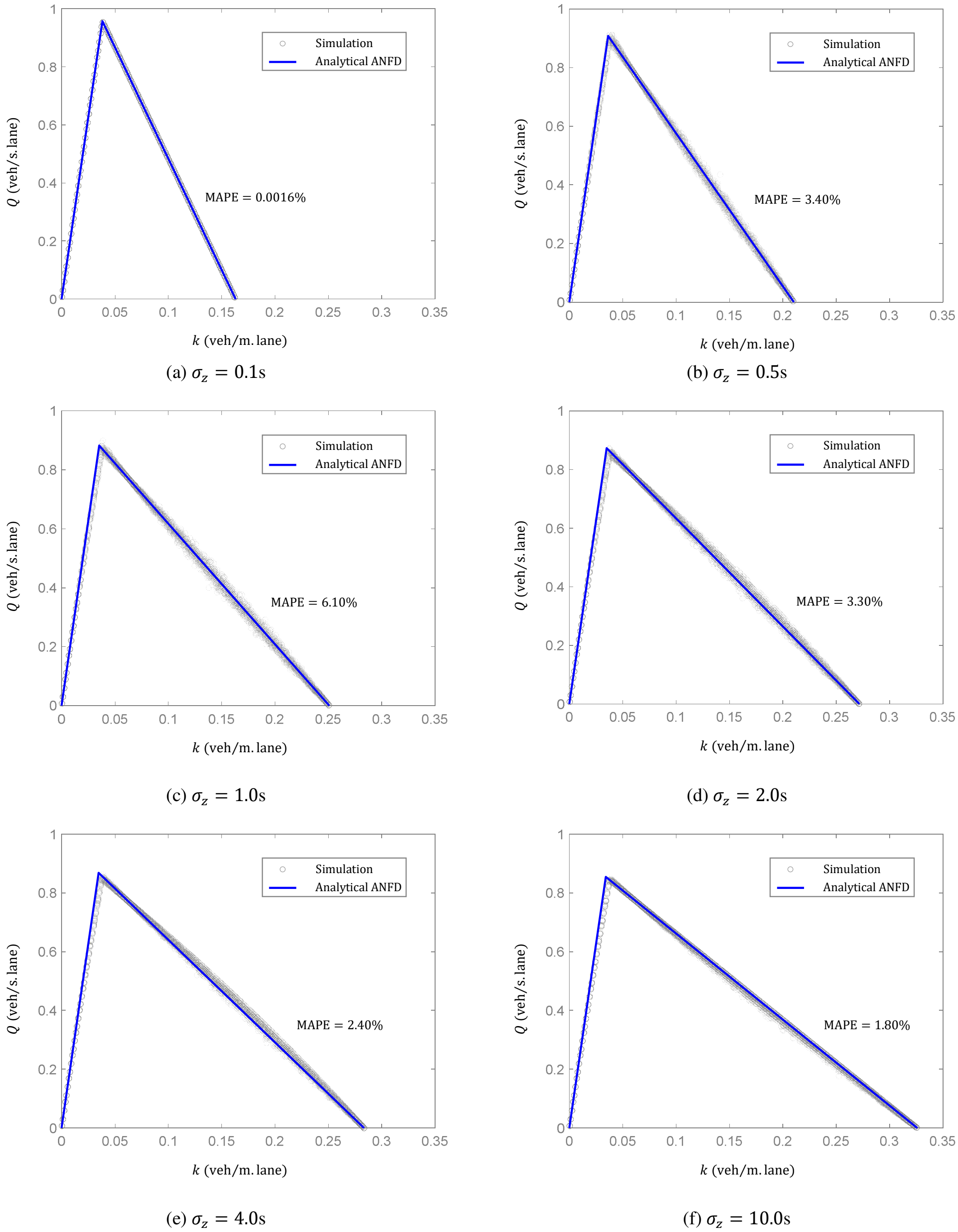

(a) $\sigma_z = 0.1$s (b) $\sigma_z = 0.5$s

(c) $\sigma_z = 1.0$s (d) $\sigma_z = 2.0$s

(e) $\sigma_z = 4.0$s (f) $\sigma_z = 10.0$s

Fig. 9. Analytical ANFD and automated double-ring simulation results

To investigate the effects of adjusting the cooperative control settings on the performance of the system, we plot the variations of the capacity (Q_m), jam density (k_j), and critical density (k_I) with the platoon size (n) and marginal gap length ($\bar{G}$) for $\sigma_z = 0.1$s in Fig. 10a-c. As discernable from the contours of Fig. 10a, the effects of increasing the platoon size and decreasing the marginal gap length on the capacity of the network are not always positive. In fact, the network capacity is maximized at the stationary point ($n^*, \bar{G}^*$), which is derived using equations (29) and (36): $n^* = 4.19$ and $\bar{G}^* = 0.06$s. The jam density, however, is an increasing function of the platoon size, but a decreasing function of the marginal gap length, as presented in Fig. 10b. The critical density is also a decreasing function of the marginal gap length, but its behavior with variations in the platoon size is not monotonic, as depicted in Fig. 10c.

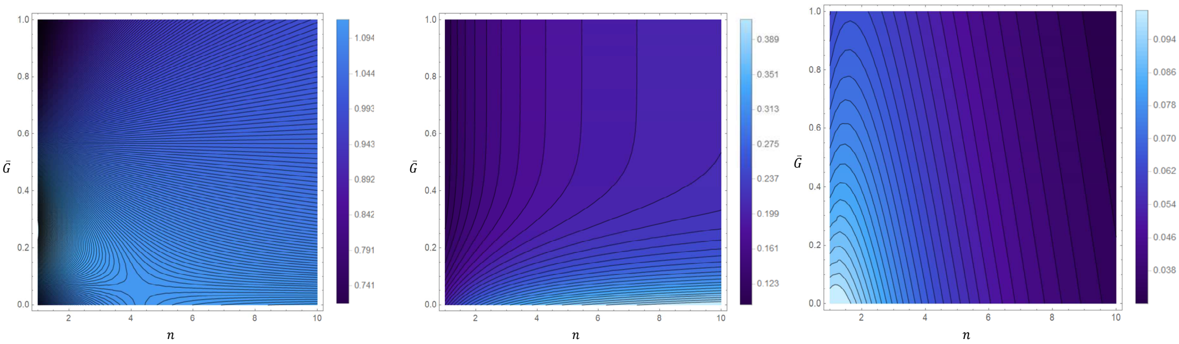

(a) Capacity, Q_m (veh/s. lane) (b) Jam density, k_j (veh/m. lane) (c) Critical density, k_I (veh/m. lane)

Fig. 10. Variations of the network performance measures with the platoon size, n (veh), and marginal gap length, $\bar{G}$ (s)

The optimal-hybrid ANFD of Fig. 11 presents the macroscopic relationship between flow and density of the automated network for the optimal platoon size, $n^* = 4.19$, and marginal gap length, $\bar{G}^* = 0.06$s. Note that altering the synchronized operation pattern of the intersections from approach-and-pass to stop-and-pass in one of the directions can improve the network performance in the highly hypercongested state ($k > k_I = 0.06$ veh/m. lane), as illustrated in Fig. 11. Comparing the ANFD of Fig. 11 with the MFD of Fig. 8 indicates that optimizing the cooperative traffic variables has increased the capacity by 138%.

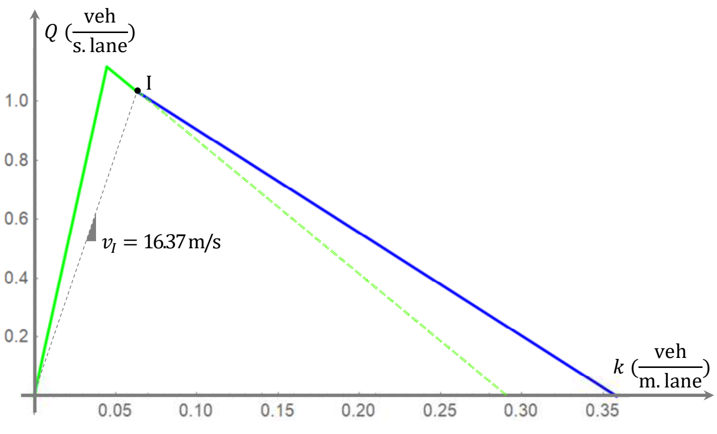

Fig. 11. Optimal-hybrid ANFD

As explained in Section 2.3, the capacity of automated networks largely depends on the platoon size and the robustness of the control system. Fig. 12a, b plot variations of the network capacity (Q_m) with the platoon size (n) and the improvement in the robustness of the control system ($P_S(\bar{G})$) as the marginal gap ($\bar{G}$) increases. As shown in Fig. 12c, the system robustness always increases with the marginal gap length, but decreases with the error standard deviation, as illustrated in Fig. 12d. Note that the effects of increasing the platoon size and improving the system robustness by increasing the length of the marginal gap on the network capacity are not always positive. Hence, it is imperative to optimize the size to the platoons and set a marginal gap of an optimal length between arrival and departure of the consecutive platoons in crossing directions to maximize the performance of automated networks.

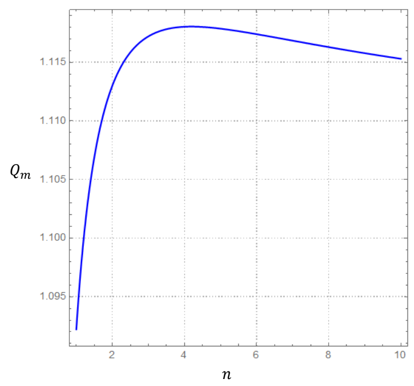

(a) Variations of the network capacity, Q_m (veh/s. lane), with the platoon size, n, for $\bar{G}^*$=0.06s and $\sigma_z = 0.1$s

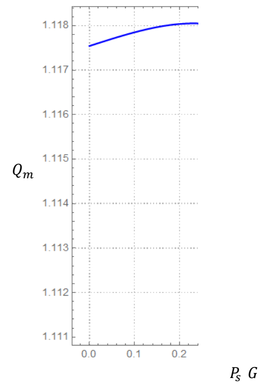

(b) Variations of the network capacity, Q_m (veh/s. lane), with improvement in the system robustness, $P_S(\bar{G})$, as the marginal gap length, $\bar{G}$, increases for $n^* = 4.19$ and $\sigma_z = 0.1$s

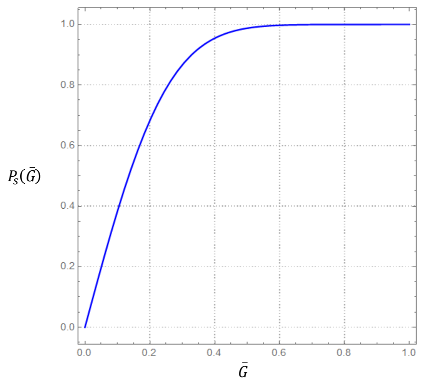

(c) Variations of the system robustness, $P_S(\bar{G})$, with marginal gap length, $\bar{G}$ (s), for $\sigma_z = 0.1$s

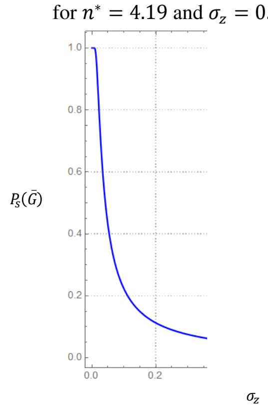

(d) Variations of the system robustness, $P_S(\bar{G})$, with σ_z (s) for $\bar{G}^*$=0.06s

Fig. 12. Automated network capacity and cooperative control robustness

6 Conclusion

Automation technology is more effective when infrastructure is integrated with traffic. In this research, we propose an optimal traffic control strategy to entirely eliminate the queue at urban intersections by making use of the headway between CAV platoons in each direction for consecutive passage of platoons in the crossing direction through the non-signalized intersection with no delay. However, the operational error in coordinating the arrivals and departures of the consecutive platoons can cause interruptions in the synchronized operation of the intersection. By formulating the synchronization failure probability, we develop a stochastic traffic model for smart urban intersections. In this model, we focus on one-way intersections with no turning traffic for simplicity of formulation. The model, however, can be further generalized by synchronizing the platoons along multilane roads and also accounting for the passing time in various turning movements and the corresponding probabilities in the formulations. Our analytical results show that the effects of increasing the platoon size and improving the system robustness by increasing the marginal gap length on the capacity of the network are not always positive. In fact, the capacity can be maximized by optimizing the size of the platoons and the length of the marginal gap. Hence, we analytically solve the optimal traffic control problem for the platoon size and marginal gap length, and derive a closed-form solution for a normal distribution of the operational error. We also introduce the ANFD as a macro-level analytical tool for modeling and optimizing the dynamics of the congestion in automated networks. The ANFD model reveals that, in the highly hypercongested state, the network performance can be significantly improved by altering the synchronized operation pattern of intersections from approach-and-pass to stop-and-pass in one of the directions. To evaluate the accuracy of the proposed model, we compare the analytical ANFD with the results of a double-ring simulation model developed for this purpose. The results indicate the high accuracy of the analytical ANFD in approximating the macroscopic relationship between the traffic variables of automated networks. Comparing the MFD and ANFD of the double-ring system also shows that optimizing the control variables increases the capacity by 138% when the error standard deviation is 0.1s.

Acknowledgments

This work was supported in part by the United States Department of Transportation (USDOT) Center for Transportation, Environment, and Community Health (CTECH), the National Science Foundation [project CMMI-1462289], and the Lloyd's Register Foundation, UK. The authors are grateful to the two anonymous reviewers for their valuable comments.

References

Amirgholy, M., Gao, H.O., 2017. Modeling the dynamics of congestion in large urban networks using the macroscopic fundamental diagram: User equilibrium, system optimum, and pricing strategies. *Transportation Research Part B: Methodological*, 104, pp.215-237.

Amirgholy, M., Shahabi, M., Gao, H.O. (2020). Traffic Automation and Lane Management: Communicant, Autonomous, and Human-Driven Vehicles. *Transportation Research Part C: Emerging Technologies* (under review).

Amoozadeh, M., Deng, H., Chuah, C.N., Zhang, H.M. and Ghosal, D., 2015. Platoon management with cooperative adaptive cruise control enabled by VANET. *Vehicular communications*, *2*(2), pp.110-123.

Aria, E., Olstam, J. and Schwietering, C., 2016. Investigation of automated vehicle effects on driver's behavior and traffic performance. *Transportation Research Procedia*, *15*, pp.761-770.

Bekiaris-Liberis, N., Roncoli, C. and Papageorgiou, M., 2016. Highway traffic state estimation with mixed connected and conventional vehicles. *IEEE Transactions on Intelligent Transportation Systems*, *17*(12), pp.3484-3497.

Biswas, S., Tatchikou, R. and Dion, F., 2006. Vehicle-to-vehicle wireless communication protocols for enhancing highway traffic safety. *IEEE communications magazine*, *44*(1), pp.74-82.

Bose, A. and Ioannou, P., 2003. Mixed manual/semi-automated traffic: a macroscopic analysis. *Transportation Research Part C: Emerging Technologies*, *11*(6), pp.439-462.

Chen, D., Ahn, S., Chitturi, M. and Noyce, D.A., 2017. Towards vehicle automation: Roadway capacity formulation for traffic mixed with regular and automated vehicles. *Transportation Research Part B: Methodological*, *100*, pp.196-221.

Daganzo, C.F., 2007. Urban gridlock: macroscopic modeling and mitigation approaches. *Transportation Research Part B*, 41 (1), 49–62.

Daganzo, C.F., Geroliminis, N., 2008. An analytical approximation for the macroscopic fundamental diagram of urban traffic. *Transportation Research Part B: Methodologica*l, 42(6), pp.771-781.

Daganzo, C.F., Gayah, V.V. and Gonzales, E.J., 2011. Macroscopic relations of urban traffic variables: Bifurcations, multivaluedness and instability. *Transportation Research Part B: Methodological*, *45*(1), pp.278-288.

Dulman, S., Nieberg, T., Wu, J. and Havinga, P., 2003, March. Trade-off between traffic overhead and reliability in multipath routing for wireless sensor networks. In *2003 IEEE Wireless Communications and Networking, 2003. WCNC 2003.* (Vol. 3, pp. 1918-1922). IEEE.

Fernandes, P. and Nunes, U., 2015. Multiplatooning leaders positioning and cooperative behavior algorithms of communicant automated vehicles for high traffic capacity. *IEEE Transactions on Intelligent Transportation Systems*, *16*(3), pp.1172-1187.

Fernandes, P. and Nunes, U., 2012. Platooning with IVC-enabled autonomous vehicles: Strategies to mitigate communication delays, improve safety and traffic flow. *IEEE Transactions on Intelligent Transportation Systems*, *13*(1), pp.91-106.

Fernandes, P. and Nunes, U., 2011, October. Algorithms for management of a multi-platooning system of IVC-enabled autonomous vehicles, with high traffic capacity. In *Intelligent Transportation Systems (ITSC), 2011 14th International IEEE Conference on* (pp. 1935-1941). IEEE.

Geroliminis, N., Haddad, J., Ramezani, M., 2013. Optimal perimeter control for two urban regions with macroscopic fundamental diagrams: A model predictive approach. *IEEE Transactions on Intelligent Transportation Systems*, 14(1), pp.348-359.

Geroliminis, N. and Levinson, D.M., 2009. Cordon pricing consistent with the physics of overcrowding. In Transportation and Traffic Theory 2009: Golden Jubilee (pp. 219-240). Springer, Boston, MA.

Geroliminis, N., Daganzo, C.F., 2008. Existence of urban-scale macroscopic fundamental diagrams: Some experimental findings. *Transportation Research Part B: Methodological*, 42(6), pp.759-770.

Geroliminis, N., Daganzo, C.F., 2007. Macroscopic modeling of traffic in cities. *Transportation Research Board 86th Annual Meeting*, No. 07-0413.

Ghiasi, A., Ma, J., Zhou, F. and Li, X., 2017. *Speed Harmonization Algorithm Using Connected Autonomous Vehicles* (No. 17-02565).

Kockelman, K., Boyles, S., Stone, P., Fagnant, D., Patel, R., Levin, M.W., Sharon, G., Simoni, M., Albert, M., Fritz, H. and Hutchinson, R., 2017. *An assessment of autonomous vehicles: traffic impacts and infrastructure needs* (No. FHWA/TX-17/0-6847-1).

Lam, S. and Katupitiya, J., 2013, July. Cooperative autonomous platoon maneuvers on highways. In *Advanced Intelligent Mechatronics (AIM), 2013 IEEE/ASME International Conference on* (pp. 1152-1157). IEEE.

Le Vine, S., Zolfaghari, A. and Polak, J., 2015. Autonomous cars: The tension between occupant experience and intersection capacity. *Transportation Research Part C: Emerging Technologies*, *52*, pp.1-14.

Li, Z., Elefteriadou, L. and Ranka, S., 2014. Signal control optimization for automated vehicles at isolated signalized intersections. *Transportation Research Part C: Emerging Technologies*, *49*, pp.1-18.

Lioris, J., Pedarsani, R., Tascikaraoglu, F.Y. and Varaiya, P., 2017. Platoons of connected vehicles can double throughput in urban roads. *Transportation Research Part C: Emerging Technologies*, *77*, pp.292-305.

Mahmassani, H.S., 2016. 50th Anniversary Invited Article—Autonomous Vehicles and Connected Vehicle Systems: Flow and Operations Considerations. *Transportation Science*, *50*(4), pp.1140-1162.

Michael, J.B., Godbole, D.N., Lygeros, J. and Sengupta, R., 1998. Capacity Analysis of Traffic Flow Over a Single-Lane Automated Highway System. *Journal of Intelligent Transportation System*, *4*(1-2), pp.49-80.

Ni, D., Li, J., Andrews, S. and Wang, H., 2010, September. Preliminary estimate of highway capacity benefit attainable with IntelliDrive technologies. In *Intelligent Transportation Systems (ITSC), 2010 13th International IEEE Conference on* (pp. 819-824). IEEE.

Ramezani, M., Haddad, J. and Geroliminis, N., 2015. Dynamics of heterogeneity in urban networks: aggregated traffic modeling and hierarchical control. *Transportation Research Part B: Methodological*, 74, pp.1-19.

Robinson, T., Chan, E. and Coelingh, E., 2010, October. Operating platoons on public motorways: An introduction to the sartre platooning programme. In *17th world congress on intelligent transport systems* (Vol. 1, p. 12).

Roncoli, C., Papageorgiou, M. and Papamichail, I., 2014. Optimal control for multi-lane motorways in presence of vehicle automation and communication systems. *IFAC Proceedings Volumes*, *47*(3), pp.4178-4183.

Shabanpour, R., Golshani, N., Shamshiripour, A. and Mohammadian, A.K., 2018. Eliciting preferences for adoption of fully automated vehicles using best-worst analysis. *Transportation Research Part C: Emerging Technologies*, 93, pp.463-478.

Shi, L. and Prevedouros, P., 2016. Autonomous and Connected Cars: HCM Estimates for Freeways with Various Market Penetration Rates. *Transportation Research Procedia*, *15*, pp.389-402.

Van Arem, B., Van Driel, C.J. and Visser, R., 2006. The impact of cooperative adaptive cruise control on traffic-flow characteristics. *IEEE Transactions on Intelligent Transportation Systems*, *7*(4), pp.429-436.

Varaiya, P., 1993. Smart cars on smart roads: problems of control. *IEEE Transactions on automatic control*, *38*(2), pp.195-207.

Yan, J. and Bitmead, R.R., 2005. Incorporating state estimation into model predictive control and its application to network traffic control. *Automatica*, *41*(4), pp.595-604.

Zhang, J. and Ioannou, P., 2004. Integrated roadway/adaptive cruise control system: safety, performance, environmental and near term deployment considerations.

Zito, R., D'este, G. and Taylor, M.A.P., 1995. Global positioning systems in the time domain: How useful a tool for intelligent vehicle-highway systems?. *Transportation Research Part C: Emerging Technologies*, *3*(4), pp.193-209

Zohdy, I., Kamalanathsharma, R., Sundararajan, S. and Kandarpa, R., 2015. Automated Vehicles from Modeling to Real World. In *Road Vehicle Automation 2* (pp. 187-191). Springer, Cham